PHYSICAL REVIEW A VOLUME 21, NUMBER 6 JUNE 1980

Dissociative ionization of H_2, D_2, and HD using electron-impact excitation

M. D. Burrows,* L. C. McIntyre, Jr., S. R. Ryan,† and W. E. Lamb, Jr.
Department of Physics, University of Arizona, Tucson, Arizona 85721
(Received 17 September 1979)

Kinetic-energy distributions of ion fragments from electron-impact bombardment of H_2, D_2, and HD have been measured at electron energies between 30 and 100 eV. In the case of H_2 these distributions at 90° are interpreted as resulting from excitation of two autoionizing states of H_2 ($^1\Sigma_g^+$ and $^1\Pi_u$) and one repulsive state of H_2^+($^2\Pi_u$). The shapes of the kinetic-energy distributions for H^+ from H_2 and D^+ from D_2 are substantially different, and a strong preference for H^+ over D^+ fragments from HD was observed.

I. INTRODUCTION

Dissociative ionization of molecular hydrogen by electron impact has been studied extensively for more than 50 years.[1-13] The data reported include measurements of thresholds, cross sections, angular distributions, and kinetic-energy distributions of the resulting protons. Although some early studies[3] were in disagreement, Dunn and Kieffer,[4] in their 1963 experiment, concluded that the measured proton kinetic-energy distributions above about 1.5 eV were in good agreement with distributions calculated using the Franck-Condon principle and "reflection approximation" assuming excitation of the $(2p\sigma_u)\,^2\Sigma_u^+$ repulsive state of H_2^+.

Subsequent measurements by Kieffer and Dunn[6] and by Van Brunt and Kieffer[7] produced evidence that whereas the $^2\Sigma_u^+$ state was a major factor in dissociative ionization, other processes were present. One piece of evidence was the existence of protons with an isotropic angular distribution at an electron bombarding energy near threshold (29 eV) for excitation of the $^2\Sigma_u^+$ state. Selection rules first stated by Dunn[14] predict that protons resulting from the $^2\Sigma_u^+$ state excited near threshold should have a $\cos^2\theta$ distribution with respect to the electron beam axis. It was suggested[6] that autoionizing states of H_2 with excitation thresholds near that of the $^2\Sigma_u^+$ H_2^+ state could contribute to the proton distribution.

In 1973 Crowe and McConkey[9] reported the observation of several resolved peaks in the proton-energy distribution between 1 and 8 eV which further pointed to the existence of processes other than $^2\Sigma_u^+$ excitation in dissociative ionization of H_2. These well-resolved peaks have not been observed by other experimenters; however, some structure has been seen in several other experiments.[10,12] Additional evidence for the complex nature of this process is provided by the structure in the D^+ distribution from electron dissociation of D_2 reported by Stockdale *et al.*,[10] the dissociative photoionization of H_2 below threshold for the $^2\Sigma_u^+$ state by Strathdee and Browning,[15] and the recent work of Köllmann[13] on H^+ from H_2 using electron bombarding energies below 29 eV. Another related work is that of Wood *et al.*,[16,17] who investigated the dissociative ionization of H_2 using fast (0.5–4 MeV) He^+ and other heavy projectiles. Their analysis of the resulting proton kinetic-energy distribution required postulating the participation of H_2 autoionizing states.

In addition to experiments involving dissociative ionization, work has been done on long-lived Rydberg-atom fragments from electron-induced dissociation of H_2, D_2, and HD.[18,19] Since the repulsive potential-energy curves which govern dissociation yielding Rydberg-atom fragments are only slightly below the corresponding curves yielding ion fragments, one might expect similar kinetic-energy distributions in these two cases. This is the prediction of the core-ion model.[20] The investigation of D_2 and HD in addition to H_2 in both ion and high-Rydberg experiments is particularly important since isotope effects may possibly provide evidence which can distinguish direct-dissociation processes from those involving autoionizing states. As recently emphasized by Van Brunt,[12] care must be used in interpreting both proton and Rydberg-atom kinetic-energy distributions taken at different observing angles since Dunn's[14] selection rules predict that the contribution of a given excited state of H_2^+ (or autoionizing state of H_2) can vary substantially with angle. As mentioned above, an important example of these selection rules is that the contribution to the proton distribution of the repulsive $^2\Sigma_u^+$ state of H_2^+ should vanish at 90° for electron energies near threshold.

Some theoretical work[21-23] has been done on doubly excited autoionizing states of H_2, and attempts[24-26] have been made to assign particular peaks in the proton spectrum of Crowe and McConkey[9] to specific autoionizing states. Hazi[24] has proposed a mechanism whereby these doubly ex-

cited states of H_2 autoionize into the dissociative continuum of the ground $^2\Sigma_g^+$ state of H_2^+.

In spite of the volume of accumulated data on this problem, the "exact nature of the dissociation mechanism involved is still not completely understood."[12] We report in this paper kinetic-energy distributions resulting from electron-induced dissociative ionization of H_2, D_2, and HD at an angle of 90° using electrons in the range 30–100 eV. A time-of-flight spectrometer with mass analysis allowed us to separate H^+ and D^+ fragments in the dissociation of HD. The H_2 data were compared with theoretical kinetic-energy distributions assuming only contributions from those states allowed at 90° by Dunn's selection rules.

II. EXPERIMENTAL METHOD

The kinetic-energy distributions reported here were obtained with a time-of-flight (TOF) method utilizing a pulsed-electron beam to excite ground-state molecules to dissociating states which produce ionic fragments. The ions then drift a known distance in a field-free region to an ion detector where their arrival stops a clock that was started by the pulsed-electron beam. The time-of-flight is stored in a multichannel analyzer and the process repeated at the rate of several kilohertz to accumulate a spectrum of the flight times. The spectrometer used in this work is similar to that described in Ref. 27, except for the addition of a new electron-bombardment ion source and the inclusion of a new mass filter-ion detector combination. The latter combination has been described elsewhere[28] in detail; however, it will be useful to outline its operation here.

The ion detector consists of an ion lens formed by a grounded plane mesh 1 cm in front of a hemispherical mesh (6.6-cm radius) held at −2400 V and a channel electron multiplier. A mask over the planar input mesh defined the sensitive area of the detector as a circle 3 cm in radius, which covers a solid angle of 7×10^{-2} sr for a 20-cm flight path.

The mass filter used in the separation of H^+ and D^+ consists of a computer-controlled, time-dependent potential barrier synchronized with the pulsed-ion source and located a distance L from it. The potential barrier is made of three closely spaced grids perpendicular to the flight path placed just in front of the detector. The two outer grids are at ground potential while the middle grid is at the potential $V(t)$. Ions with mass m arriving at the mass filter at a time t after the source pulse have a kinetic energy $mL^2/2t^2$ so that if the potential barrier $V(t)$ varies as $m_0L^2/2et^2 \equiv k/t^2$, ions with $m > m_0$ will pass through the filter to the detector and those with $m < m_0$ will be reflected. To achieve mass analysis, spectra are accumulated with scale factors k corresponding to cutoff masses m_0 and m_0' and later subtracted to give a TOF spectrum of all ions with mass between m_0 and m_0'. A set of nine m_0 values, covering the range $0.5 \leq m_0 \leq 3.2$ amu in nearly equal increments, was used to acquire spectra of H^+ and D^+ ions. A minicomputer that serves as a multichannel analyzer to accumulate the TOF spectra is programmed to periodically change the scale factor k of the retarding potential, storing the data corresponding to each k in a separate sector of memory. The nine mass spectra are accumulated by changing the mass cutoff scale factor every 30 msec which, in conjunction with the 4 kHz electron pulse repetition rate, serves to average any long-term drifts in the experimental parameters over all the spectra.

The electron-gun pulse duration and TOF channel width were 0.1 μsec. The flight path from the center of the ion source to the middle mass filter grid was 18.9 cm, while the total path to the ion detector was 19.9 cm. The bombarding electron beam, the inlet gas stream, and the TOF drift path are mutually perpendicular to minimize the effects of electron-impact momentum transfer and the thermal velocity of the parent molecule. Because the cathode of the electron gun is directly heated, the total spread in electron-impact energies is approximately 2 eV. The time average electron bombarding current was 10^{-8} A for 4 kHz repetition rate. The spatial extent of the electron-bombardment interaction region (≈4 mm), which was determined by an electron-gun aperture of 4 mm and a 2-mm gas inlet tube, is the major limitation in the TOF energy resolution. The interaction region is relatively open and free of surfaces that can accumulate charge; nevertheless, space charge, contact potentials, and accumulated charge can alter the kinetic energy of the ions. These effects are generally small and can be measured by accumulating a TOF spectrum of He^+ ions produced by electron-impact bombardment of He gas. Although the kinetic-energy distribution of the He ions should be approximately thermal, the He^+ spectrum typically consisted of a peak centered at 0.3 eV with a full width at half maximum (FWHM) of 0.1 eV. The peak was observed to vary from 0.1 to 0.3 eV in a random fashion and to completely disappear on a few occasions. No correlation between the energy of the He^+ ions and the gas pressure, electron current, or voltage could be ascertained. Hence, the ion kinetic energies measured in these experiments are possibly higher than the true values by 0.2 to 0.3 eV. Since the emphasis in this study is on high-energy frag-

ments, this residual potential in the source is not of major importance, although it can probably be reduced by careful source design.

III. RESULTS AND DISCUSSION

A. H_2

Kinetic-energy distribution of H^+ fragments from H_2 obtained in the manner described above at electron energies of 50 and 100 eV are presented in Fig. 1. Also shown on this figure for comparison are the 90° data of Van Brunt[12] taken at 75-eV electron energy and the Rydberg-atom data of Carnahan and Zipf.[19] Although all these distributions have similar shapes, our data peaks at a lower energy than the previous results. Our distribution peaks at about 4.5 eV whereas Van Brunt[12] observes the peak at about 5.5 eV. This discrepancy of about 1 eV is substantial; however, it is not particularly disturbing in view of our estimated uncertainty in energy scale of approximately 0.3 eV. This estimate is based on the combined uncertainties in flight path, knowledge of time zero, contact potentials, and effects of the electron beam. We have no reason to believe that our apparatus discriminates against higher-energy ions, since in other applications we have obtained good agreement with other measurements. Examples of such agreement are our results[29, 30] on N^+ ions from N_2 and H^+ and H_2^+ ions from CH_4 and C_2H_6. The results reported here for H_2 and

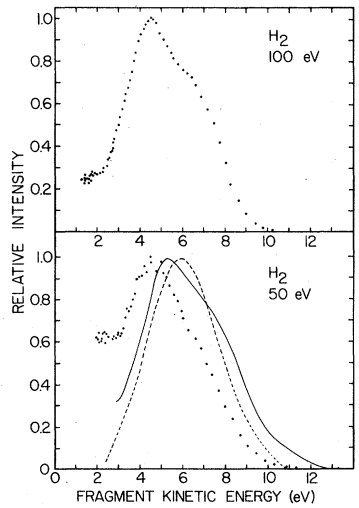

FIG. 1. Kinetic-energy distributions of H^+ fragments from H_2 at the indicated electron-impact energies. The observation angle was 90°. The dotted curves are our results. The solid line curve is the 75-eV, 90° data of Van Brunt (Ref. 12). The dashed curve is the Rydberg-atom distribution of Carnahan and Zipf (Ref. 19) taken at 50 eV and 90°.

D_2 were taken both with and without the mass-filter grids in place. No substantial differences were observed.

Since the predicted distribution from $^2\Sigma_u^+$ excitation (as well as Van Brunt's data[12] at 23°) peaks at 8 eV, it is clear that this is not the dominant process at 90°. It appears that Dunn's selection rules may be approximately valid quite far above threshold in this case. In an attempt to identify the contributing processes at 90°, we have fit our measured kinetic-energy distributions between 30 and 50 eV with calculated distributions using only excited states of H_2^+ and H_2 allowed by Dunn's selection rules. The states with nonvanishing H^+ yield at 90° under this assumption are Σ_g^+, Π_u, and Δ_g states. These states consist of both autoionizing states and those purely repulsive states which yield H^+ fragments in the separated atom limit. The purely repulsive states are the $(2p\pi_u)\,^2\Pi_u$ state of H_2^+ and higher-energy states of H_2^+ lying in the manifold of states below the doubly ionized state corresponding to $H_2^{+\,2}$. Currently, the known autoionizing states of H_2 with the appropriate symmetry are the $Q_1\,^1\Sigma_g^+$, $Q_1\,^1\Pi_u$, and $Q_2\,^1\Pi_u$ states described by Bottcher and Docken,[22] Hazi,[25] and Bottcher.[26] A Q_2 state can autoionize to either the $^2\Sigma_g^+$ ground state or the $^2\Sigma_u^+$ repulsive state of H_2^+; a Q_1 state can only autoionize via the ground state. Since Bottcher's[26] results indicate that the autoionization width for the $Q_2\,^1\Pi_u$ state is about two orders of magnitude smaller than either of the Q_1 states, we have chosen to neglect its contribution and fit the data using only the $Q_1\,^1\Sigma_g^+$ and $Q_1\,^1\Pi_u$ states of H_2 and the $(2p\pi_u)\,^2\Pi_u$ state of H_2^+. Contributions from the manifold of H_2^+ states above the $(2p\pi_u)^2\Pi_u$ state have likewise been neglected since they begin to contribute only above 40 eV and are expected to yield kinetic-energy distributions similar to the $2p\pi_u$ state.

Potential-energy curves[22, 25, 26, 31] of some states in H_2 and H_2^+ including the three states mentioned above are shown in Fig. 2. The calculated proton kinetic-energy distributions resulting from excitation of these states are shown in Fig. 3. The Franck-Condon principle and the reflection approximation were used to obtain the distribution resulting from the $(2p\pi_u)\,^2\Pi_u$ state of H_2^+. The method described by Hazi[23] was used for the autoionizing states. In the latter case the kinetic-energy distribution is largely determined by the behavior of the autoionizing width $\Gamma(R)$ as a function of internuclear distance. In both cases the cross section for excitation was assumed to increase linearly with excess electron energy above threshold[32] and was averaged over the 2-eV spread in the electron pulse. Thresholds for these three states are $Q_1\,^1\Sigma_g^+$ (24.5 eV), $Q_1\,^1\Pi_u$

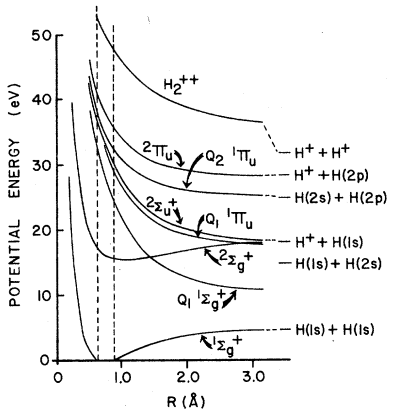

FIG. 2. Potential-energy curves for some states of H_2, H_2^+, and H_2^{++}. The dashed vertical curve indicates the approximate extent of the Franck-Condon region. The $Q_1\ ^1\Pi_u$ curve was taken from Hazi (Ref. 25); the $Q_1\ ^1\Sigma_g^+$ and $Q_2\ ^1\Pi_u$ curves are from Bottcher and Docken (Ref. 22) and Bottcher (Ref. 26); the remainder are from Sharp (Ref. 31).

(29.2 eV), and $2p\pi_u\ ^2\Pi_u$ (35.7 eV).

The decay width $\Gamma(R)$ and potential-energy curve for the $Q_1\ ^1\Sigma_g^+$ state were taken from Bottcher and Docken[22] using Hazi's[23] analytic approximation for $\Gamma(R)$. For the $Q_1\ ^1\Pi_u$ state the potential curve obtained by Hazi[25] was used in conjunction with a $\Gamma(R)$ given (in a.u.) by $0.1\exp(-0.744)(R-R_m)^2$, where R_m is 4 bohr. This is an approximate analytic expression to Bottcher's[26] results.[33] With these decay widths and 35-eV electron-impact energies, our calculations predict that 25% of the initial $Q_1\ ^1\Sigma_g^+$ population decays via autoionization while 45% of the initial $Q_1\ ^1\Pi_u$ population undergoes autoionization. The measured proton-energy distributions and the calculated composite curves at 30-, 35-, 40-, 45-, and 50-eV electron energy are shown in Fig. 4. The relative contributions to the proton distribution of the three states at each electron energy are given in Table I. These numbers indicate the relative areas of each kinetic-energy distribution

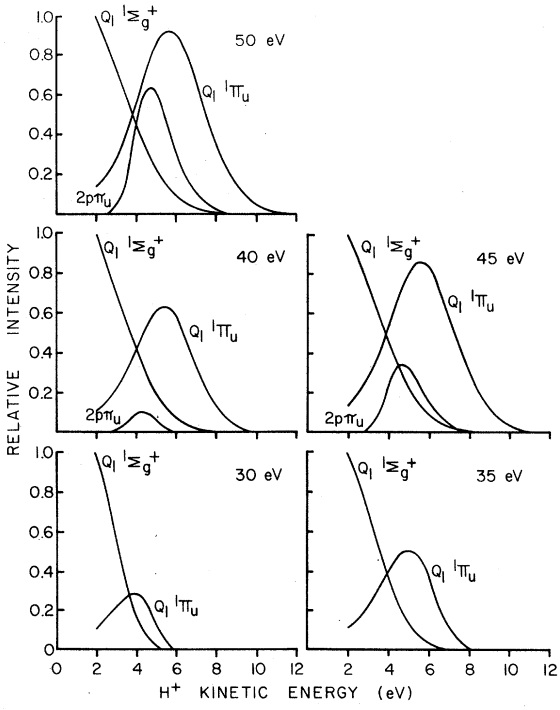

FIG. 3. Calculated kinetic-energy distributions of H^+ from H_2 at several electron bombarding energies. The area under each curve (above 2 eV) is proportional to its contribution to the total H^+ yield as shown in the calculated distributions in Fig. 4.

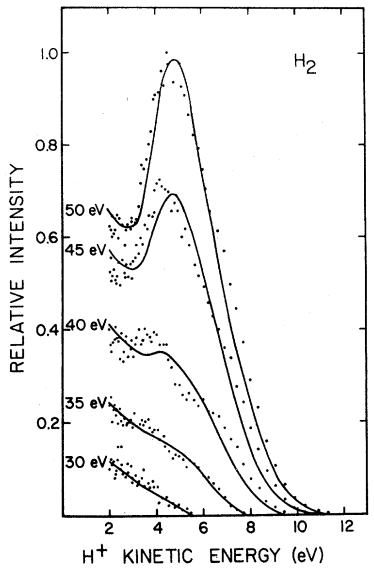

FIG. 4. Measured kinetic-energy distributions (at 90°) of H^+ from H_2 at several electron bombarding energies (dotted curves). The solid line curves are calculated distributions using the relative contributions of two autoionizing states of H_2 and one repulsive state in H_2^+ as indicated in Table I.

TABLE I. Fractional contribution of the indicated states to the H^+ yield from H_2 above 2 eV for several electron bombarding energies computed from a fit to the experimental distributions.

Electron impact energy (eV)	$Q_1\ ^1\Sigma_g^+$	$Q_1\ ^1\Pi_u$	$(2p\pi_u)\ ^2\Pi_u$
30	0.65	0.35	
35	0.52	0.48	
40	0.43	0.53	0.04
45	0.33	0.55	0.12
50	0.28	0.51	0.21

that must be added to obtain the fit to the observed data shown in Fig. 4.

The resulting fits are reasonably good, leading to the conclusion that at 90° and for electron energies below 50 eV, the observed proton-energy distributions can be explained by considering only the $Q_1\,^1\Sigma_g^+$ and $Q_1\,^1\Pi_u$ autoionizing state of H_2 and the $2p\pi_u$ repulsive state of H_2^+. Because of the many other possible contributing states it is difficult to judge the uniqueness of this explanation. Probably the most significant observation is the absence of a strong $(2p\sigma_u)\,^2\Sigma_u^+$ state contribution far above threshold.

B. D_2 and HD

Kinetic-energy distributions of D^+ ions from D_2 at 50 and 100 eV electron energy are shown in Fig. 5. The data of Stockdale *et al.*[10] and the Rydberg-atom data of Carnahan and Zipf[19] are also shown for comparison. It is seen that while all three distributions have a similar shape with two obvious features (at about 4 and 7 eV) the relative amplitude of these features is not the same in the different experiments. The discrepancy between our data and that of Stockdale *et al.*[10] is substantial. Stockdale *et al.*[10] estimate a 10% uncertainty in their energy scale, which in view of our estimated uncertainty of 0.3 eV is not sufficient to explain the difference in relative ion yield at ion kinetic energies of 6–10 eV. We can offer no explanation of this difference.

Whereas the total range in kinetic energies accessible to H^+ fragments from H_2 and D^+ fragments from D_2 are comparable, the shapes of the respective distributions are noticeably different. At 100-eV impact energies, the high-energy shoulder in the D^+ kinetic-energy distribution is better defined and higher in amplitude than the corresponding shoulder in the H^+ distribution. At 50-eV excitation energies, this shoulder is still clearly present in the D^+ but noticeably weaker in the H^+ distribution. These differences are consistent with a substantial dissociative autoionization contribution. The relative amounts of autoionization should be greater in D_2 than in H_2, since the autoionization probability is inversely proportional to the relative velocity of the fragments.

Our results for H^+ and D^+ energy distributions from HD are shown in Fig. 6. At 100 eV the Rydberg-atom kinetic-energy distributions of Carnahan and Zipf[19] show two features at about 9- and 15-eV total released kinetic energy. The high-energy feature is not apparent in our ion distributions. Furthermore, the Rydberg-atom dis-

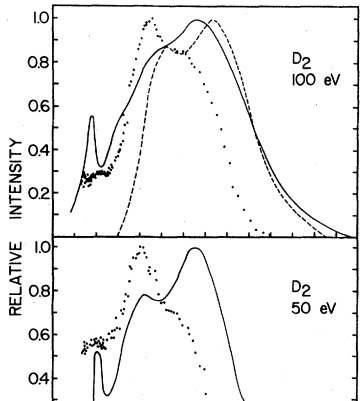

FIG. 5. Kinetic-energy distributions of D^+ fragments from D_2 at the indicated electron-impact energies. The observation angle was 90°. The dotted curves are our results. The solid line curves are the 90° data of Stockdale *et al.* (Ref. 10) taken at the same electron energies. The dashed-line curve is the Rydberg-atom data of Carnahan and Zipf (Ref. 19) taken with 100-eV electrons and 90° observation angle.

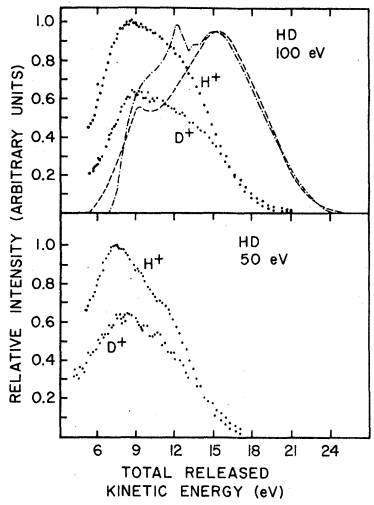

FIG. 6. Total released kinetic-energy distribution for H^+ and D^+ fragments from HD at 50- and 100-eV electron energies. The observation angle was 90°. The $H^+(D^+)$ kinetic energy is obtained by multiplying the indicated energy by $\frac{2}{3}$ ($\frac{1}{3}$). The Rydberg-atom data of Carnahan and Zipf (Ref. 19) at 100 eV and 90° are shown as dashed [H(HR)] and dot-dashed [D(HR)] curves. These Rydberg-atom curves were calculated from Fig. 6(b) of Ref. 19 and are separately normalized; therefore, they do not reflect the 2:1 ratio of H(HR) to D(HR) reported in that work. The sharp feature on the D(HR) distribution is an artifact of a smoothing and time-to-energy conversion process and is not a reproducible feature of the actual distribution (Ref. 19).

tributions extend to approximately 24 eV of total released kinetic energy, while our ion distributions extend to only 21 eV.

Thus many more Rydberg fragments than ion fragments are detected with relatively large kinetic energies. Our ion results indicate that excitation of the $(2p\sigma_u)\,^2\Sigma_u^+$ state of H_2^+, D_2^+, or HD^+ at 90° observation angles is still relatively weak for 100-eV impact energies, as would be expected if Dunn's selection rules are still approximately valid. For high-Rydberg fragments, however, there are numerous Rydberg states of H_2, situated immediately below the $(2p\sigma_u)\,^2\Sigma_u^+$ state of H_2^+, which can yield high-Rydberg-fragment distributions peaking at about 15 eV of total released kinetic energy. A number of these states, corresponding to $H(1s)+H(nl)$ in the separated atom limit, can be excited consistent with Dunn's selection rules. These states may, in part, be responsible for the larger numbers of high-kinetic-energy Rydberg fragments observed where the corresponding ion intensity is weak. Since a large fraction of the ions originate from autoionizing states, where the ejected electron carries off a substantial portion of the released kinetic energy, the Rydberg distributions should peak at higher kinetic energies than the ion distributions, as has been noted by Schiavone *et al.*[18]

Carnahan and Zipf[19] found a preference for H (HR) over D (DR) fragments of a factor of 2 which is slightly larger than that observed in the present ion fragment results. Carnahan and Zipf also observed a preference for fast H(2S) over fast D(2S) fragments by a factor of 1.2, although Czuchlewski and Ryan[34] observed equal H(2S) and D(2S) contributions. The exact mechanism responsible for this preferential formation of H^+ and H neutrals is difficult to ascertain since it is generally assumed that the fragment pairs $H^+ + D(nl)$ and $D^+ + H(nl)$ will be formed with equal probabilities from a given dissociating state. While the semiclassical models of dissociative autoionization predict isotope effects, these effects depend on the reduced mass rather than the relative nuclear masses.

In summary, we observe significant isotope effects for dissociative ionization in the H_2-D_2-HD molecular family, consistent with a large dissociative autoionization contribution for fragments observed at 90° with respect to the bombarding electron beam. For impact energies of 35 eV or less, dissociative autoionization involving the $Q_1\,^1\Sigma_g^+$ and $Q_1\,^1\Pi_u$ states of H_2 appears to be the dominant ionization channel. At higher impact energies of 40 to 50 eV, the $(2p\pi_u)\,^2\Pi_u$ directly dissociating state of H_2^+ makes a significant contribution. At 50 and 100-eV excitation energies dissociative autoionization processes are still important ionization channels, as evidenced by the different shapes of the kinetic energy distributions for H^+ from H_2 and D^+ from D_2.

ACKNOWLEDGMENTS

The authors would like to thank Joe Spezeski, Otto Kalman, and Bruce Kittams for valuable assistance in checking some of the data appearing in this work. This research was sponsored by the Air Force Office of Scientific Research, Air Force Systems Command, USAF, under Grant No. 75-2864.

*Present address: Air Force Weapons Lab, Kirtland Air Force Base, Albuquerque, New Mexico 87117.
†Present address: University of Oklahoma, Norman, Oklahoma 73019.

[1]W. Bleakney, Phys. Rev. 35, 1180 (1930).
[2]W. W. Lozier, Phys. Rev. 36, 1285 (1930).
[3]D. P. Stevenson, J. Am. Chem. Soc. 82, 5961 (1960).
[4]G. H. Dunn and L. J. Kieffer, Phys. Rev. 132, 2109 (1963).
[5]D. Rapp, P. Englander-Golden, and D. D. Briglia, J. Chem. Phys. 42, 4081 (1965).
[6]L. J. Kieffer and G. H. Dunn, Phys. Rev. 158, 61 (1967).
[7]R. J. Van Brunt and L. J. Kieffer, Phys. Rev. A 2, 1293 (1970).
[8]A. Crowe and J. W. McConkey, J. Phys. B 6, 2088 (1973).
[9]A. Crowe and J. W. McConkey, Phys. Rev. Lett. 31, 192 (1973).
[10]J. A. D. Stockdale, U. E. Anderson, A. E. Carter, and L. Deleanu, J. Chem. Phys. 63, 3886 (1975).
[11]K. Köllmann, Int. J. Mass Spectrom. Ion Phys. 17, 261 (1975).
[12]R. J. Van Brunt, Phys. Rev. A 16, 1309 (1977).
[13]K. Köllmann, J. Phys. B 11, 339 (1978).
[14]G. H. Dunn, Phys. Rev. Lett. 8, 62 (1962).
[15]S. Strathdee and R. Browning, J. Phys. B 9, L505 (1976).
[16]R. M. Wood, A. K. Edwards, and M. F. Stever, Phys. Rev. A 15, 1433 (1977).
[17]A. K. Edwards, R. M. Wood, and M. F. Stever, Phys. Rev. A 16, 1385 (1977).
[18]J. A. Schiavone, K. C. Smyth, and R. S. Freund, J. Chem. Phys. 63, 1043 (1975).
[19]B. L. Carnahan and E. C. Zipf, Phys. Rev. A 16, 991 (1977).
[20]S. E. Kupriyanov, Zh. Eksp. Teor. Fiz. 55, 460 (1968) [Sov. Phys.—JETP 28, 240 (1969)].
[21]T. F. O'Malley, J. Chem. Phys. 51, 322 (1969).

[22]C. Bottcher and K. Docken, J. Phys. B 7, L5 (1974).
[23]A. U. Hazi, J. Chem. Phys. 60, 4358 (1974).
[24]A. U. Hazi, Chem. Phys. Lett. 25, 259 (1974).
[25]A. U. Hazi, J. Phys. B 8, L262 (1975).
[26]C. Bottcher, J. Phys. B 7, L352 (1974).
[27]S. R. Ryan, S. J. Czuchlewski, and M. V. McCusker, Phys. Rev. A 16, 1892 (1977).
[28]M. D. Burrows, S. R. Ryan, W. E. Lamb, Jr., and L. C. McIntyre, Jr., Rev. Sci. Instrum. 50, 1278 (1979).
[29]M. D. Burrows, Ph.D. thesis, University of Arizona, 1979 (unpublished).
[30]M. D. Burrows, S. R. Ryan, W. E. Lamb, Jr., and L. C. McIntyre, Jr., J. Chem. Phys. 71, 4931 (1979).
[31]T. E. Sharp, At. Data 2, 119 (1971).
[32]S. Geltman, Phys. Rev. 102, 171 (1956).
[33]Since Bottcher's calculations for the $Q_1\,^1\Pi_u$ state yielded a potential curve situated above the $2p\sigma_u$ state of H_2^+, there is some uncertainty as to the validity of his $\Gamma(R)$. For this reason the analytic expression for Γ indicated in the text was used for computational simplicity. Both forms of $\Gamma(R)$, however, possess a maximum at approximately 4 bohr and yield a proton kinetic-energy distribution peaked at 5.5 eV.
[34]S. J. Czuchlewski and S. R Ryan, Bull. Am. Phys. Soc. 18, 688 (1973); S. J. Czuchlewski, Ph.D. thesis, Yale University, 1973 (unpublished).